Hindawi
Journal of Nanomaterials
Volume 2018, Article ID 3150351, 6 pages
https://doi.org/10.1155/2018/3150351

Research Article

Biodistribution and Acute Toxicity of Intravenous Multifunctional ^{125}I-Radiolabeled Fe_3O_4-Ag Heterodimer Nanoparticles in Mice

Bin Zhang,[1] **Jing Zhu**,[2] **Hongwei Gu**,[3] **and Shengming Deng**[1]

[1]*Department of Nuclear Medicine, The First Affiliated Hospital of Soochow University, Suzhou, 215006 Jiangsu, China*
[2]*Department of Applied Chemistry, Anhui Agricultural University, Hefei, 230036 Anhui, China*
[3]*Key Laboratory of Organic Synthesis of Jiangsu Province, College of Chemistry, Chemical Engineering and Materials Science & Collaborative Innovation Center of Suzhou Nano Science and Technology, Soochow University, Suzhou 215123, China*

Correspondence should be addressed to Shengming Deng; dshming@163.com

Received 9 August 2018; Revised 25 September 2018; Accepted 11 October 2018; Published 11 November 2018

Academic Editor: Angelo Taglietti

Fe_3O_4-$Ag^{125}I$ heterostructured radionuclide nanoparticles (NPs) have been developed as a novel type of dual-modality imaging agents for single-photon emission computerized tomography (SPECT) and magnetic resonance imaging (MRI). However, the biodistribution and toxicity of Fe_3O_4-$Ag^{125}I$ NPs remain largely unknown. Therefore, we investigated the biodistribution and biological action of Fe_3O_4-$Ag^{125}I$ NPs in mice by acute toxicity experiments (exposures over 7 days). The bioaccumulation of Fe_3O_4-$Ag^{125}I$ NPs was studied via *in vivo* experiments. The serum biochemistry and hematology were analyzed to reveal potential functional changes. The histopathological changes were observed by using an electron microscope. Biodistribution analysis revealed that Fe_3O_4-$Ag^{125}I$ NPs were mainly accumulated in the liver and spleen. The activities of liver enzymes (ALT and AST) were increased in Fe_3O_4-$Ag^{125}I$ NP-challenged groups compared with the control groups. Collectively, liver and spleen were the major target organs for accumulation of Fe_3O_4-$Ag^{125}I$ NPs. Damage of liver tissue was observed in the Fe_3O_4-$Ag^{125}I$ NP-challenged groups compared with the control groups. Further studies on surface coating of Fe_3O_4-Ag with targeted materials are highly necessary for safe medical applications of Fe_3O_4-AgNPs as dual-modality imaging agents.

1. Introduction

In recent years, a great deal of attention has been paid to silver nanoparticles (AgNPs) since they are used as popular antibacterial and antifungal agents in the light of an enormously increasing bacterial resistance against repeatedly and excessively used classical antibiotics. AgNPs can effectively eliminate bacteria at a relatively low concentration [1–3]. Besides antimicrobial ability, AgNPs are effective in the field of photothermal cancer therapy and/or surface-enhanced Raman spectroscopy [4].

Magnetic iron oxide (Fe_3O_4) NPs have been widely used in many important fields due to their unique characteristics, such as biochemical properties, superparamagnetism and low price [5–8]. Fe_3O_4-Ag heterodimer NPs possess magnetic functionality and antimicrobial ability at the same time [2].

Our group has successfully developed Fe_3O_4-$Ag^{125}I$ heterostructured radionuclide NPs as novel dual-modality imaging agents for magnetic resonance imaging (MRI) and single-photon emission computerized tomography (SPECT) [9]. The Fe_3O_4-$Ag^{125}I$ heterostructured radionuclide NPs demonstrate high radiolabeling efficiency and clearly reduced T_2-MRI signal intensity.

We aimed to apply this material to medical imaging. However, no study has investigated the distribution and toxicity of Fe_3O_4-AgNPs in animals. Moreover, previous studies show inconsistent results, indicating that the distribution and toxicity of Fe_3O_4 or Ag NPs are highly dependent on the various factors, such as shape, size, coating agent of the

NPs, duration after drug administration, and animal gender [10–15]. Therefore, we investigated the biodistribution and toxicity of Fe_3O_4-$Ag^{125}I$ NPs in mice after intravenous injection. The bioaccumulation of Fe_3O_4-$Ag^{125}I$ NPs was studied via *in vivo* experiments. The serum biochemistry and hematology were analyzed to reveal potential functional changes. The histopathological changes were observed by using an electron microscope.

2. Materials and Methods

2.1. Ethics Statement. Male Kunming mice (6 weeks of age) were purchased from the Center for Experimental Animal of Soochow University. Animal experiments were preapproved by the institutional review board and the Experimental Animal Center of the First Affiliated Hospital of Soochow University. All SPECT scans were performed under general anesthesia, and all efforts were made to minimize animal suffering.

2.2. Materials. All the reagents for the synthesis of Fe_3O_4-AgNPs were purchased from Sigma-Aldrich. ^{125}I was obtained from Chengdu Gaotong Isotope Corporation (Chengdu, China). All other chemicals were prepared with analytical-grade reagents dissolved in deionized water prepared by LabWater (Shanghai Hejie Technology Co. Ltd.).

2.3. Synthesis of Fe_3O_4-$Ag^{125}I$ NPs. Fe_3O_4-$Ag^{125}I$ NPs were synthesized as previously reported [9]. Briefly, the Fe_3O_4 NPs were synthesized by thermal decomposition of iron-oleate complex, and then the AgNPs were grown onto the cubic Fe_3O_4 NPs by adding the silver acetate into the reaction system. Subsequently, the Fe_3O_4-AgNPs were functionalized by hydrophilic mPEG-LA polymers and phase transferred from hexane to water. Finally, Fe_3O_4-$Ag^{125}I$ NPs were produced by reacting the Ag component of the heterostructured NPs with ^{125}I.

The labeling efficiency and radiochemical purity were analyzed using paper chromatography. The fractions containing ^{125}I-labeled Fe_3O_4-Ag were determined using a gamma counter to calculate the radiolabeling yield (%). The solution was filtered through a 0.22 μm pore-size membrane in order to avoid potential bacterial and dust particles for *in vivo* studies.

2.4. Biodistribution of Fe_3O_4-$Ag^{125}I$ NPs. Kunming mice ($n = 5$ per time point) were intravenously injected with Fe_3O_4-$Ag^{125}I$ NPs (100 μL/4.92–6.99 MBq) via the tail vein once daily and sacrificed by exsanguination under ether anesthesia at 1, 2, 8, 24, and 48 h after injection. Blood samples (approximately 100 μL each) were collected via retroorbital bleeding, and main organs, such as the blood, lung, brain, kidney, liver, pancreas, spleen, stomach, thyroid, intestine, bone, and muscle, were dissected from anesthetized mice and weighed at 1, 2, 8, 24, and 48 h postinjection. The radioactivity of the tissue was measured in a γ-counter (Shanghai Nucleus Research Institute Rihuan Photoelectric Instrument Co. Ltd.). The uptake in organs was calculated as the proportion of injected dose per gram of tissue (%ID/g).

2.5. In Vivo SPECT Imaging. SPECT scans were performed using the IRIX (Philips, Netherlands) equipped with high-resolution low-energy parallel-hole collimator. Briefly, after injection of Fe_3O_4-$Ag^{125}I$ NPs, mice were anesthetized using isoflurane. The SPECT scans were performed at various time points. Images were acquired with 1×10^5 counts on a 128×128 matrix. The energy peak for the camera was set to 37 keV, and the energy window was set to peak energy ±30%, which was 26–48 keV.

2.6. Serum Biochemistry and Hematology. The mice were sacrificed after injection of Fe_3O_4-$Ag^{125}I$ NPs (40 mg/mL) for seven consecutive days. The blood was collected from the retroorbital sinus. For hematological analysis, the blood samples were combined with EDTA-3K for anticoagulation. The hematological measurements were performed using an automated hematology analyzer (BC-5800, Mindray Co., Shenzhen, China) following the standard protocols.

For serum biochemistry analysis, the blood samples were centrifuged at 3000 rpm for 15 min within 1 h, and the supernatant was collected. All the biochemical parameters were determined on a clinical automatic chemistry analyzer (Chemray360, Rayto Co., Shenzhen, China) following the standard protocols.

2.7. Transmission Electron Microscopy (TEM). For TEM analysis of the spleen, heart, liver, and kidney, small pieces of tissue samples (~1 mm^3) were fixed in 2.5% glutaraldehyde solution overnight and washed with phosphate-buffered saline (PBS). Postfixation was performed with 1% osmium tetroxide for 2 h. Then, the samples were washed with PBS and dehydrated with a graded series of alcohols (50%, 70%, 80%, 95%, and 100%), followed by rinsing with acetone. Ultrathin sections from each tumor sample were prepared and examined under JEOL-JEM-2100F TEM operating at 200 kV.

2.8. Statistical Analysis. The results were expressed as the mean ± standard deviation (SD). Data were analyzed by one-way ANOVA and Student's t-test. $p < 0.05$ was considered as statistically significant. All statistical tests were two sided.

3. Results

3.1. Radioiodination of Fe_3O_4-AgNPs. The radiolabeling efficiency of Fe_3O_4-$Ag^{125}I$ heterostructured NPs was 95.57% ± 2.06%, and the radiochemical purity was 91.99% ± 0.32% after 24 h.

A TEM image (Figure 1) confirmed that the average size of Fe_3O_4-AgNPs was 24.53 ± 2.99 nm. The addition of a radionuclide into the Fe_3O_4-AgNPs did not change the morphology of the samples.

3.2. Biodistribution of Fe_3O_4-$Ag^{125}I$ NPs in Mice. Figure 2 presents the biodistribution data of Fe_3O_4-$Ag^{125}I$ NPs in different organs at various time points postinjection. The uptake of Fe_3O_4-$Ag^{125}I$ was high in the liver (31.98 ± 3.74%ID/g at 1 h after injection, 31.00 ± 9.42%ID/g at 2 h after injection, 22.51 ± 4.57%ID/g at 8 h after injection, 5.79 ± 4.24%ID/g at 24 h after injection, and 4.48 ± 2.20%ID/g at

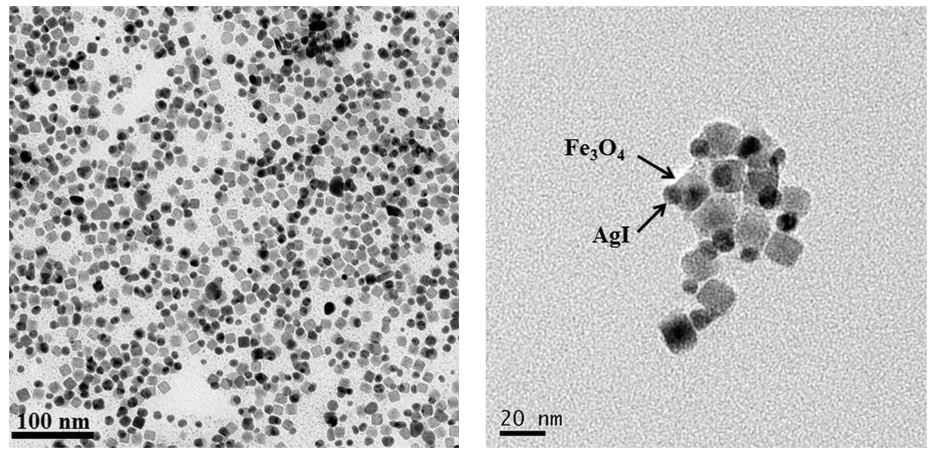

(a) (b)

Figure 1: TEM images of Fe_3O_4-$Ag^{125}I$ heterodimer NPs.

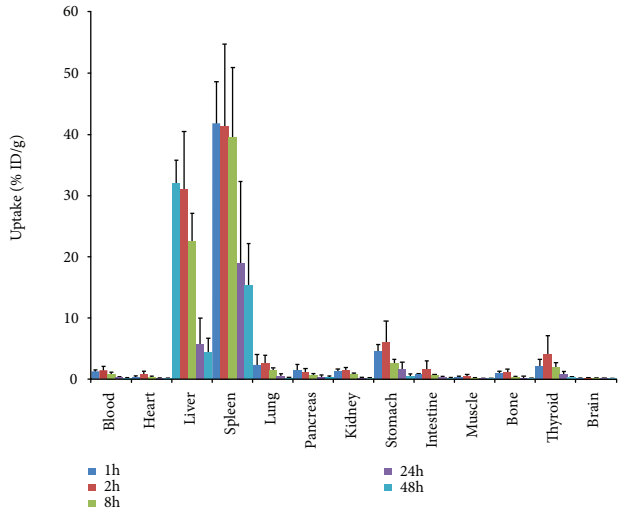

Figure 2: Biodistribution of Fe_3O_4-$Ag^{125}I$ in mice over time reported as % ID ($n = 5$).

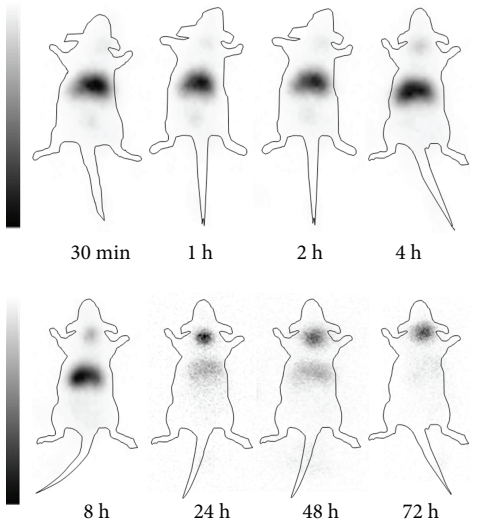

Figure 3: Representative static whole-body SPECT imaging of Fe_3O_4-$Ag^{125}I$ localization in mouse at 0.5, 1, 2, 4, 8, 24, 48, and 72 h after injection.

48 h after injection) and spleen (41.87 ± 6.73%ID/g at 1 h after injection, 41.41 ± 13.32%ID/g at 2 h after injection, 39.49 ± 11.37%ID/g at 8 h after injection, 19.07 ± 13.22%ID/g at 24 h after injection, and 15.34 ± 6.82%ID/g at 48 h after injection). These findings indicated that the injected ^{125}I-labled conjugates were mainly taken up by the reticuloendothelial system (RES).

A moderate level of radioactivity was accumulated in the thyroid (2.15 ± 1.04%ID/g at 1 h after injection, 4.21 ± 2.90%ID/g at 2 h after injection, 1.94 ± 0.74%ID/g at 8 h after injection, 0.83 ± 0.44%ID/g at 24 h after injection, and 0.29 ± 0.10%ID/g at 48 h after injection) and stomach (4.52 ± 1.15%ID/g at 1 h after injection, 6.16 ± 3.29%ID/g at 2 h after injection, 2.67 ± 0.51%ID/g at 8 h after injection, 1.58 ± 1.16%ID/g at 24 h after injection, and 0.56 ± 0.24%ID/g at 48 h after injection). These accumulations were probably attributed to free ^{125}I released *in vivo*.

A low level of radioactivity was present in the brain (0.11 ± 0.04%ID/g at 1 h after injection, 0.15 ± 0.11%ID/g at 2 h after injection, 0.07 ± 0.02%ID/g at 8 h after injection, 0.04 ± 0.02%ID/g at 24 h after injection, and 0.02 ± 0.01%ID/g at 48 h after injection, respectively) and muscle (0.35 ± 0.17%ID/g at 1 h after injection, 0.50 ± 0.26%ID/g at 2 h after injection, 0.20 ± 0.06%ID/g at 8 h after injection, 0.08 ± 0.04%ID/g at 24 h after injection, and 0.05 ± 0.02%ID/g at 48 h after injection).

3.3. SPECT Imaging Studies. Mice administered with Fe_3O_4-$Ag^{125}I$ NPs were subjected to SPECT imaging. Figure 3 shows representative images of mice obtained at 0.5, 1, 2, 4, 8, 24, 48, and 72 h postinjection.

The activity level in the abdominal region (particularly the spleen and liver) was high in the first five static images, which was generally consistent with the results of *in vivo* biodistribution studies, indicating that the injected Fe_3O_4-$Ag^{125}I$ NPs were mainly sequestered by the RES.

Table 1: Haematological and serum biochemistry parameters of the mice exposed to Fe_3O_4-$Ag^{125}I$. Data represent means ± SD ($n = 5$).

	ALB (g/L)	ALT (U/L)	AST (U/L)	ALP (U/L)	Ur (mmol/L)	Cr (μmol/L)	WBC (10^9/L)	RBC (10^{12}/L)	HB (g/L)	PLT (10^9/L)
Control	27.32 ± 0.98	15.32 ± 10.34	189.33 ± 32.11	71.12 ± 22.96	8.03 ± 1.69	21.52 ± 4.74	3.94 ± 0.74	8.40 ± 0.93	143.00 ± 5.66	759.50 ± 65.76
Fe_3O_4-$Ag^{125}I$	26.14 ± 2.48	30.93 ± 14.41*	256.35 ± 56.28*	69.63 ± 15.05	10.27 ± 1.98	35.16 ± 30.21	3.81 ± 1.39	7.21 ± 0.42	120.50 ± 3.54	629.00 ± 131.52

*$p < 0.05$ compared with control group. ALB: albumin; ALT: alanine aminotransferase; AST: aspartate aminotransferase; ALP: alkaline phosphatase; Ur: urea; Cr: creatinine; WBC: white blood cell count; RBC: red blood cell count; HB: hemoglobin; PLT: platelet.

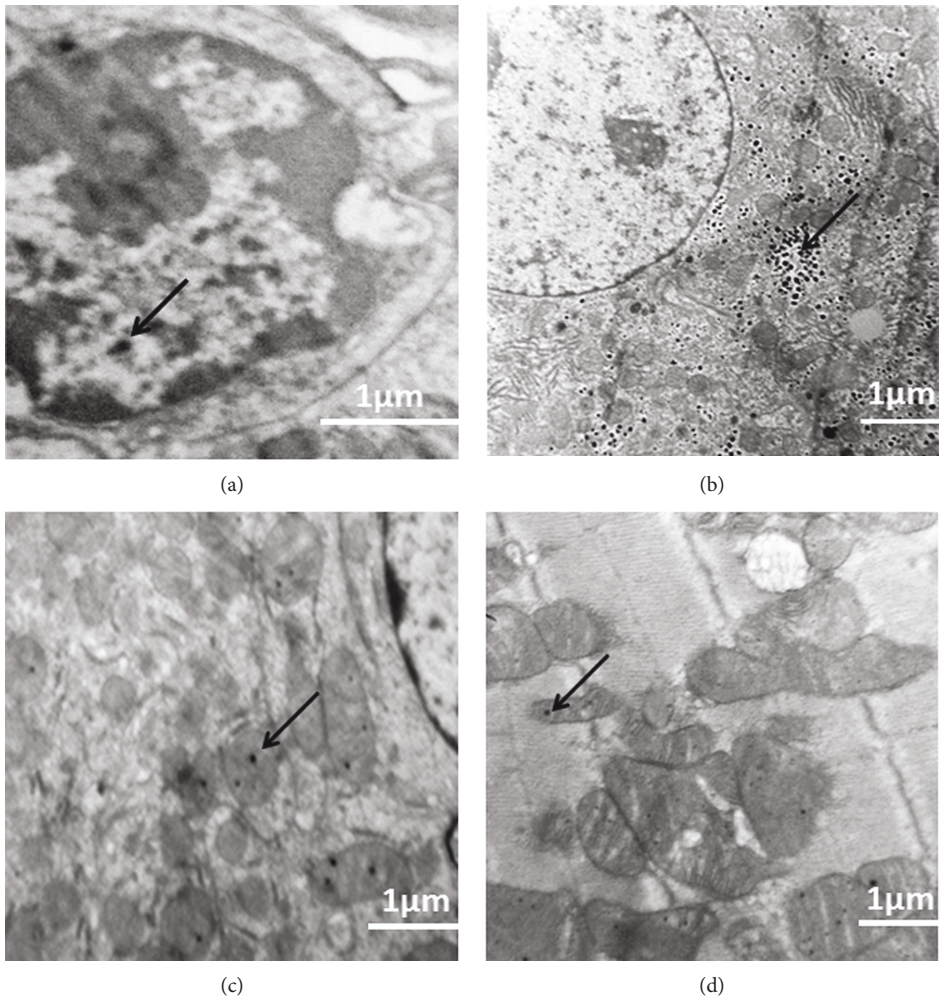

Figure 4: TEM images of the spleen, heart, liver, and kidney of Fe_3O_4-$Ag^{125}I$ NPs-treated mice: (a) spleen, (b) liver, (c) kidney, and (d) heart. Arrows in black color show NPs.

Little radioactivity was observed in the thyroid region during the early imaging procedure. However, there were slight increases in thyroid at the end of the imaging procedure, suggesting that this compound was deiodinated *in vivo* just as the results of biodistribution.

3.4. Toxicity Evaluations. Haematological and serum biochemistry parameters were analyzed after exposure to Fe_3O_4-$Ag^{125}I$ NPs. Table 1 lists the data.

Most parameters remained within the normal ranges at 7 days after the intravenous injection of Fe_3O_4-$Ag^{125}I$ NPs. Significant changes were only observed for alanine aminotransferase (ALT) and aspartate aminotransferase (AST).

3.5. TEM Analysis. TEM analysis was performed on the spleen, heart, liver, and kidney from the Fe_3O_4-$Ag^{125}I$ NPs-administered mice and negative control mice (Figure 4). The results demonstrated that the Fe_3O_4-$Ag^{125}I$ NPs agglomerated in the spleen. In the liver, Fe_3O_4-$Ag^{125}I$ NPs were scattered throughout the parenchyma. In line with the result of biodistribution, less Fe_3O_4-$Ag^{125}I$ NPs were detected in the heart and kidney.

4. Discussion

During the past few decades, there are increasing applications of AgNPs in various fields. However, AgNPs have several shortcomings, including agglomeration, easy oxidation, low penetration into tissue, and cytotoxicity [16, 17]. Iron oxide NPs can add a magnetic functionality and prevent agglomeration to AgNPs. It has been reported that the bactericidal efficiency of Fe_3O_4-AgNPs is stronger than Fe_2O_3-Ag heterodimers or plain Ag [18]. Despite the advantages of Fe_3O_4-AgNPs, the biodistribution and toxicity of Fe_3O_4-AgNPs remain largely unexplored.

In the present study, we systematically investigated the biodistribution of Fe_3O_4-AgNPs in mice after intravenous injection by noninvasive nuclear imaging techniques. Our study confirmed that the majority of Fe_3O_4-$Ag^{125}I$ NPs were accumulated in the spleen and liver, and such pattern could be attributed to uptake by the B cells and macrophages in the spleen and the Kupffer cells in the liver, which are part of the mononuclear phagocyte system. These results were consistent with some previous studies on biodistribution of nontargeted AgNPs and Fe_3O_4 NPs [19–22]. Chrastina and Schnitzer have radiolabeled AgNPs with ^{125}I to track the *in vivo* tissue uptake of AgNPs after systemic administration by biodistribution analysis and SPECT imaging. Their results have also revealed the uptake of AgNPs in the liver and spleen [23].

Recently, toxicity of Fe_3O_4 NPs or AgNPs has been widely studied. Fe_3O_4 NPs are generally considered as biocompatible, safe, and nontoxic materials. Median lethal dose (LD-50) of the uncoated Fe_3O_4 NPs is 300–600 mg Fe/kg body weight [24]. However, the toxicity of AgNPs based on *in vivo* studies is controversial. Maneewattanapinyo et al. have investigated the acute oral toxicity of AgNPs by *in vivo* experiments and found that the LD-50 of colloidal AgNPs is greater than 5000 mg/kg body weight [25]. Another study has also revealed that no obvious changes in serum chemistry, hematology, and histopathology are found after SD rats are administered with up to 36 mg/kg AgNPs by oral gavage for 13 weeks [14]. However, other studies have demonstrated that short-term administration of AgNPs can significantly increase ALT or/and AST [15, 26, 27]. Tiwari et al. have investigated the toxic effect of various doses of AgNPs on Wistar rats and indicated that AgNPs at lower dose (<10 mg/kg) are safe, while its higher dose (>20 mg/kg) is toxic [28]. Recently, Ghaseminezhad et al. have compared the cytotoxicities of AgNPs and Ag/Fe_3O_4 nanocomposites to human fibroblasts and found that Ag/Fe_3O_4 nanocomposites are less cytotoxic than AgNPs [29]. The Ag/Fe_3O_4 nanocomposites show lower release of Ag ions and less ROS production compared with AgNPs. In the present study, the activities of liver enzymes (ALT and AST) were increased in the Fe_3O_4-$Ag^{125}I$ NP-challenged groups compared with the control groups, indicating that liver tissues were damaged following administration of Fe_3O_4-$Ag^{125}I$ NPs.

Some studies have suggested that the toxicity of AgNPs depends on surface capping. It has been demonstrated that polysaccharide-coated AgNPs induce more severe damages compared with uncoated AgNPs [30], whereas carbon-coated AgNPs are less cytotoxic towards macrophages [31]. Therefore, in order to develop the Fe_3O_4-$Ag^{125}I$ heterostructured radionuclide NPs as dual-modality imaging agents, NPs need to be coated with special compounds in the future. Additional studies are required in order to reshape the surface of Fe_3O_4-Ag to modify their characteristics.

Collectively, our present study investigated the biodistribution and acute toxicity of ^{125}I-radiolabeled Fe_3O_4-Ag heterodimer NPs in mice. We found that the liver and spleen were the major target organs for the accumulation of Fe_3O_4-$Ag^{125}I$ NPs. Damage of liver tissue was observed in the Fe_3O_4-$Ag^{125}I$ NP-challenged groups compared with the control groups. Further studies on surface coating of Fe_3O_4-Ag with targeted materials are highly necessary for safe medical applications of Fe_3O_4-AgNPs as dual-modality imaging agents.

Data Availability

The data used to support the findings of this study are available from the corresponding author upon request.

Conflicts of Interest

The authors declare no conflict of interest.

Acknowledgments

This work was financially supported by National Natural Science Foundation of China (Nos. 81601522, 51702004), Natural Science Foundation of Jiangsu Province (No. BK20160348), Medical Youth Talent Project of Jiangsu Province (No. QNRC2016749), Science and Technology Project for the Youth of Suzhou (No. kjxw2015004), Anhui Provincial Natural Science Foundation (No. 1808085QE158), and Introduction and Stabilization of Talent Projects of Anhui Agricultural (No. yj2017-06).

References

[1] P. Dallas, V. K. Sharma, and R. Zboril, "Silver polymeric nanocomposites as advanced antimicrobial agents: classification, synthetic paths, applications, and perspectives," *Advances in Colloid and Interface Science*, vol. 166, no. 1-2, pp. 119–135, 2011.

[2] M. Guzman, J. Dille, and S. Godet, "Synthesis and antibacterial activity of silver nanoparticles against gram-positive and gram-negative bacteria," *Nanomedicine*, vol. 8, no. 1, pp. 37–45, 2012.

[3] S. Shrivastava, T. Bera, A. Roy, G. Singh, P. Ramachandrarao, and D. Dash, "Characterization of enhanced antibacterial effects of novel silver nanoparticles," *Nanotechnology*, vol. 18, no. 22, pp. 225103–225112, 2007.

[4] R. Prucek, J. Tuček, M. Kilianová et al., "The targeted antibacterial and antifungal properties of magnetic nanocomposite of iron oxide and silver nanoparticles," *Biomaterials*, vol. 32, no. 21, pp. 4704–4713, 2011.

[5] L. Gao, K. Fan, and X. Yan, "Iron oxide nanozyme: a multifunctional enzyme mimetic for biomedical applications," *Theranostics*, vol. 7, no. 13, pp. 3207–3227, 2017.

[6] H. Podrouzkova, V. Feitova, R. Panovsky, J. Meluzin, and M. Orban, "Superparamagnetic iron oxide-enhanced magnetic resonance for imaging cardiac inflammation. A minireview," *Biomedical Papers of the Medical Faculty of the University Palacky, Olomouc, Czech Republic*, vol. 159, no. 3, pp. 378–381, 2015.

[7] M. Swierczewska, S. Lee, and X. Chen, "Inorganic nanoparticles for multimodal molecular imaging," *Molecular Imaging*, vol. 10, no. 1, pp. 3–16, 2011.

[8] S. Deng, W. Zhang, B. Zhang et al., "Radiolabeled cyclic arginine-glycine-aspartic (RGD)-conjugated iron oxide nanoparticles as single-photon emission computed tomography (SPECT) and magnetic resonance imaging (MRI) dual-modality agents for imaging of breast cancer," *Journal of Nanoparticle Research*, vol. 17, no. 1, p. 19, 2015.

[9] J. Zhu, B. Zhang, J. Tian et al., "Synthesis of heterodimer radionuclide nanoparticles for magnetic resonance and single-photon emission computed tomography dual-modality imaging," *Nanoscale*, vol. 7, no. 8, pp. 3392–3395, 2015.

[10] L. Yang, H. Kuang, W. Zhang et al., "Size dependent biodistribution and toxicokinetics of iron oxide magnetic nanoparticles in mice," *Nanoscale*, vol. 7, no. 2, pp. 625–636, 2015.

[11] R. C. Popescu, E. Andronescu, and A. M. Grumezescu, "In vivo evaluation of Fe_3O_4 nanoparticles," *Romanian Journal of Morphology and Embryology*, vol. 55, Supplement 3, pp. 1013–1018, 2014.

[12] K. S. Siddiqi, A. Husen, and R. A. K. Rao, "A review on biosynthesis of silver nanoparticles and their biocidal properties," *Journal of Nanobiotechnology*, vol. 16, no. 1, p. 14, 2018.

[13] D. W. Han, Y. I. Woo, M. H. Lee, J. H. Lee, J. Lee, and J. C. Park, "*In-vivo* and *in-vitro* biocompatibility evaluations of silver nanoparticles with antimicrobial activity," *Journal of Nanoscience and Nanotechnology*, vol. 12, no. 7, pp. 5205–5209, 2012.

[14] M. D. Boudreau, M. S. Imam, A. M. Paredes et al., "Differential effects of silver nanoparticles and silver ions on tissue accumulation, distribution, and toxicity in the Sprague Dawley rat following daily oral gavage administration for 13 weeks," *Toxicological Sciences*, vol. 150, no. 1, pp. 131–160, 2016.

[15] H. Wen, M. Dan, Y. Yang et al., "Acute toxicity and genotoxicity of silver nanoparticle in rats," *PLoS One*, vol. 12, no. 9, article e0185554, 2017.

[16] N. G. Durmus and T. J. Webster, "Eradicating antibiotic-resistant biofilms with silver-conjugated superparamagnetic iron oxide nanoparticles," *Advanced Healthcare Materials*, vol. 2, no. 1, pp. 165–171, 2013.

[17] A. Taglietti, C. R. Arciola, A. D'Agostino et al., "Antibiofilm activity of a monolayer of silver nanoparticles anchored to an amino-silanized glass surface," *Biomaterials*, vol. 35, no. 6, pp. 1779–1788, 2014.

[18] M. E. F. Brollo, R. López-Ruiz, D. Muraca, S. J. A. Figueroa, K. R. Pirota, and M. Knobel, "Compact $Ag@Fe_3O_4$ core-shell nanoparticles by means of single-step thermal decomposition reaction," *Scientific Reports*, vol. 4, no. 1, article 6839, 2014.

[19] L. Yang, H. Kuang, W. Zhang, Z. P. Aguilar, H. Wei, and H. Xu, "Comparisons of the biodistribution and toxicological examinations after repeated intravenous administration of silver and gold nanoparticles in mice," *Scientific Reports*, vol. 7, no. 1, p. 3303, 2017.

[20] A. Ashraf, R. Sharif, M. Ahmad et al., "In vivo evaluation of the biodistribution of intravenously administered naked and functionalised silver nanoparticles in rabbit," *IET Nanobiotechnology*, vol. 9, no. 6, pp. 368–374, 2015.

[21] Q. Feng, Y. Liu, J. Huang, K. Chen, J. Huang, and K. Xiao, "Uptake, distribution, clearance, and toxicity of iron oxide nanoparticles with different sizes and coatings," *Scientific Reports*, vol. 8, no. 1, p. 2082, 2018.

[22] H. Arami, A. Khandhar, D. Liggitt, and K. M. Krishnan, "In vivo delivery, pharmacokinetics, biodistribution and toxicity of iron oxide nanoparticles," *Chemical Society Reviews*, vol. 44, no. 23, pp. 8576–8607, 2015.

[23] A. Chrastina and J. E. Schnitzer, "Iodine-125 radiolabeling of silver nanoparticles for *in vivo* SPECT imaging," *International Journal of Nanomedicine*, vol. 5, pp. 653–659, 2010.

[24] S. Wada, L. Yue, K. Tazawa et al., "New local hyperthermia using dextran magnetite complex (DM) for oral cavity: experimental study in normal hamster tongue," *Oral Diseases*, vol. 7, no. 3, pp. 192–195, 2001.

[25] P. Maneewattanapinyo, W. Banlunara, C. Thammacharoen, S. Ekgasit, and T. Kaewamatawong, "An evaluation of acute toxicity of colloidal silver nanoparticles," *The Journal of Veterinary Medical Science*, vol. 73, no. 11, pp. 1417–1423, 2011.

[26] A. K. Patlolla, D. Hackett, and P. B. Tchounwou, "Silver nanoparticle-induced oxidative stress-dependent toxicity in Sprague-Dawley rats," *Molecular and Cellular Biochemistry*, vol. 399, no. 1-2, pp. 257–268, 2015.

[27] M. S. Heydrnejad, R. J. Samani, and S. Aghaeivanda, "Toxic effects of silver nanoparticles on liver and some hematological parameters in male and female mice (*Mus musculus*)," *Biological Trace Element Research*, vol. 165, no. 2, pp. 153–158, 2015.

[28] D. K. Tiwari, T. Jin, and J. Behari, "Dose-dependent in-vivo toxicity assessment of silver nanoparticle in Wistar rats," *Toxicology Mechanisms and Methods*, vol. 21, no. 1, pp. 13–24, 2011.

[29] S. M. Ghaseminezhad, S. A. Shojaosadati, and R. L. Meyer, "Ag/Fe_3O_4 nanocomposites penetrate and eradicate *S. aureus* biofilm in an *in vitro* chronic wound model," *Colloids and Surfaces B: Biointerfaces*, vol. 163, pp. 192–200, 2018.

[30] M. Ahamed, M. Karns, M. Goodson et al., "DNA damage response to different surface chemistry of silver nanoparticles in mammalian cells," *Toxicology and Applied Pharmacology*, vol. 233, no. 3, pp. 404–410, 2008.

[31] R. P. Nishanth, R. G. Jyotsna, J. J. Schlager, S. M. Hussain, and P. Reddanna, "Inflammatory responses of RAW 264.7 macrophages upon exposure to nanoparticles: role of ROS-NFκB signaling pathway," *Nanotoxicology*, vol. 5, no. 4, pp. 502–516, 2011.